Solid-State Electronics 200 (2023) 108521

Contents lists available at ScienceDirect

Solid State Electronics

journal homepage: www.elsevier.com/locate/sse

Prediction of the evolution of defects induced by the heated implantation process: Contribution of kinetic Monte Carlo in a multi-scale modeling framework ☆

P.L. Julliard [a,b,*], A. Johnsson [c], N. Zographos [d], R. Demoulin [b], R. Monflier [b], A. Jay [b], O. Er-Riyahi [b], F. Monsieur [a], S. Joblot [a], F. Deprat [a], D. Rideau [a], P. Pichler [c], A. Hémeryck [b], F. Cristiano [b]

[a] STMicroelectronics, Crolles, France
[b] LAAS-CNRS, Université de Toulouse, CNRS, Toulouse, France
[c] Fraunhofer Institute for Integrated Systems and Device Technology (IISB), Erlangen, Germany
[d] Synopsys Switzerland LLC, Zurich, Switzerland

ARTICLE INFO

Keywords:
Kinetic Monte Carlo
Process simulations
Heated implantation
Multi-scale modeling

ABSTRACT

Extended defects formed as a result of heated implantation and thermal annealing are studied using transmission electron microscopy and kinetic Monte Carlo simulations. We highlight the relevance of using kinetic Monte Carlo approach to provide information to continuum-scale simulations as well as the value of integrating data from atomic-scale calculations for its calibration.

1. Introduction

The leakage current in transistors is known to increase in the presence of extended defects such as {311} and dislocation loops [1]. Extended defects can be related to the implantation and annealing process. Thus, innovative process conditions to reduce the defects concentration, such as heated implantation, are being explored [2]. To assist in the optimization of the heated implantation process, kinetic Monte Carlo (KMC) is an efficient methodology as it takes temperature into account [3] and is integrated in the state-of-the-art technology computer-aided design (TCAD) software Sentaurus Process [4]. This KMC methodology has already been shown to be accurate for simulating extended defects in annealing following room temperature (RT) implantations [5].

In this work, KMC as implemented in [4] is used to investigate the defects remaining after the heated implantation followed by an annealing process, from small interstitial clusters (SMICs) to the formation of dislocation loops (DLs). The simulation results are compared to transmission electron microscopy (TEM) for three implantation conditions where the temperature varies. The experimental results (Section 2) reveal two distinct regimes of defect formation for which different levels of modeling are required as a function of temperature (Section 3), i.e., a hybrid approach coupling the KMC and continuum solvers of [4] for low implantation temperatures and, for high implantation temperature, a full KMC scheme.

2. Experimental results

Three Si wafers were implanted with arsenic using a heated implantation process, at three temperatures: RT, 150 °C and 500 °C.

For each temperature, the implantation was performed in two steps: a first implantation at 180 keV with a dose of 10^{14} cm^{-2} and a second implantation at 100 keV with a dose of 8×10^{13} cm^{-2}. An identical annealing treatment was applied for the three implanted wafers (see Table 1). These as-implanted wafers were analyzed by TEM (Fig. 1(a)) and after the annealing cycle (Fig. 1(b) and (c)).

In Fig. 1(a), showing the material after implantation, we observe an amorphous layer at RT, and a damaged material at 150 °C and 500 °C. After annealing (Fig. 1-(b) and (c)), for both RT and 150 °C implantations, DLs are observed. Implantation at high temperature (500 °C) exhibits a different kind of defects, i.e., extended {311} defects. The depth at which the DLs and {311} defects are observed depends on the as-implanted damages. In the case of amorphizing implantations (RT), the defects are localized close to the amorphous/crystalline interfaces

☆ The review of this paper was arranged by Francisco Gamiz.

* Corresponding author at: STMicroelectronics, Crolles, France.
E-mail address: pierre-louis.julliard@st.com (P.L. Julliard).

https://doi.org/10.1016/j.sse.2022.108521

Available online 22 November 2022

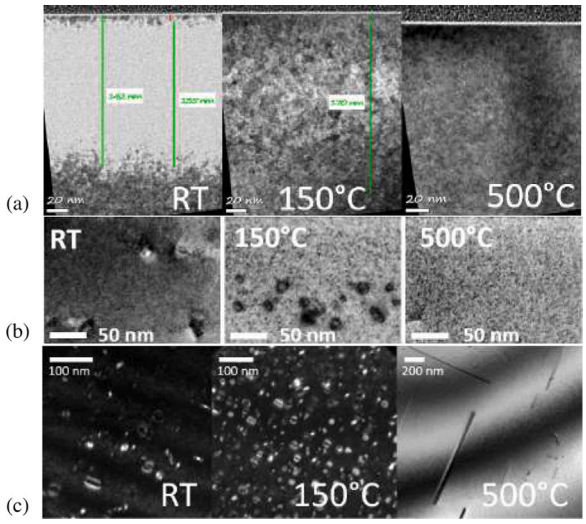

Fig. 1. TEM analysis of As implanted Si wafers at three temperatures: RT, 150 °C and 500 °C from left to right. (a) as-implanted wafer, and (b) and (c) after the annealing sequence as given in Table 1. In (b) TEM images are viewed in cross-section and in (c) in plane-view.

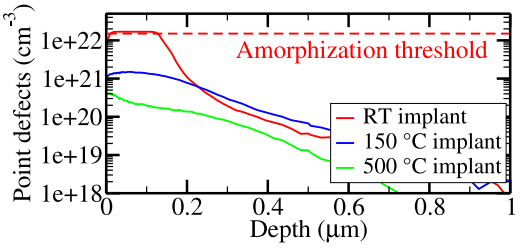

Fig. 2. KMC simulations of total point defects concentration as-implanted in the RT, 150 °C and 500 °C cases.

(so called End-of-Range defects) as can be seen in Fig. 1(a). In the non-amorphizing cases (150 °C and 500 °C), the defects are localized at the mean projected range of the implanted species, closer to the surface than the defects of the RT implantation.

3. Simulations results

3.1. KMC first results

The KMC model as implemented in [4] takes the dose rate and the implantation temperature into account. These parameters have an impact on the interstitial-vacancies recombination and thus must be considered in the case of heated implantation. The KMC model of [4] predicts the formation of an amorphous layer after the RT implantation and no amorphous layer in the 150 °C and 500 °C cases (Fig. 2). These results are consistent with the TEM observation in Fig. 1. The predicted amorphous layer position (from 16 nm to 122 nm) in the RT case is also in fair agreement with the one observed in TEM where the full amorphous material is observed between 10 nm and 130 nm.

The KMC can also be used to simulate the defects evolution during the annealing sequence. In the case of RT and 150 °C implantations, the KMC predicts the formation of DLs after the annealing in good consistency with the TEM images. The KMC provides an estimate of the density of interstitials trapped in the DLs close to the TEM count for RT implantation, but it overestimates it by 50 % for the 150 °C implantation (Table 2). The KMC in the RT and 150 °C cases reproduces experimental observation but requires a long computational time. In the case of the 500 °C implantation, the KMC predicts DLs at the end

Table 1
Annealing sequence following the implantations at RT, 150 °C and 500 °C.

Annealing steps	1	2	3	4	5	6
Temperature (°C)	625	750	700	625	800	750
Time (min)	120	60	210	52	30	60

Table 2
Interstitial densities trapped in DLs. TEM count is compared to the predictions of two simulations methods: KMC simulation of the implantation and the annealing (full KMC) and an approach using KMC for the implantation and continuum model for the annealing (Hybrid).

I in DLs (cm^{-2})	TEM	full KMC	Hybrid
RT	1.4×10^{14}	1.2×10^{14}	0.94×10^{14}
150 °C	1.6×10^{14}	2.3×10^{14}	3.9×10^{14}

of the annealing sequence. This result is not consistent with the {311} defects observed in TEM. Moreover, the density of interstitials trapped in defects is 5×10^{12} in TEM measurements and is 1.5×10^{14} in the KMC simulations.

Here, we observe the limits of the KMC approach, whether computational or related to the catalog of events. To reproduce, in the most efficient way, the two experimental trends observed at the end of annealing, i.e, DLs in RT and 150 °C implantations and {311} in 500 °C implantation, two modeling approaches have been used : a coupling between the KMC and continuum solvers of [4] for RT and 150 °C implantation temperatures (Section 3.2). For high temperature implantation (500 °C), a full KMC simulation was performed based on the results of both molecular dynamics (MD) simulation [6] and own density functional theory (DFT) calculations for a detailed calibration of interstitial clusters (Section 3.3 and 3.4).

3.2. Using hybrid KMC-continuum solver for RT and 150 °C implantations

To take advantage of the speed of continuum simulations without having to calibrate its parameters from TEM experiments, a hybrid approach combining KMC for implantation and the first annealing ramp and continuum simulations for annealing was performed. The excess interstitials present in the amorphous pockets (interstitials-vacancies clusters) and interstitial clusters obtained at the end of the KMC simulations are then converted into a continuous data field associated with I_2 species, i.e a cluster composed of 2 interstitials (in the following I_n refers to a cluster of n interstitials). In the region where there are more vacancies than interstitials, the excess vacancies are converted into a continuous field of free vacancies. A continuous model, using the two moments approach of [4] for SMICs, {311}, DLs and vacancies based clusters evolution, is used to simulate the annealing. Fig. 3 shows the evolution of the density of interstitials trapped in DLs and in {311} defects. It can be seen that at the end of the annealing, the simulation predicts that most interstitials are trapped in DLs, in good agreement with TEM observations. Here, the interstitial densities in DLs simulated are of the same order of magnitude as in the TEM count, while the densities of interstitials in DLs in the 150 °C case is overestimated (see Table 1). The use of the KMC-continuum switching divides the computational time by a factor 8 compared to a full KMC simulation using the same box size.

3.3. Dependence of SMIC size for 500 °C implantations

At 500 °C heated implantation, the KMC predicts the formation of DLs, in disagreement with TEM where {311} are observed.

Since the annealing sequences are the same for the three wafers, we consider that the difference resulting in the {311} formation comes from the implantation step. The difference between the number of interstitials and vacancies in the as-implanted wafers was estimated to be 8.61×10^{13} cm^{-2} for the 150 °C case and 8.86×10^{13} cm^{-2} for 500 °C

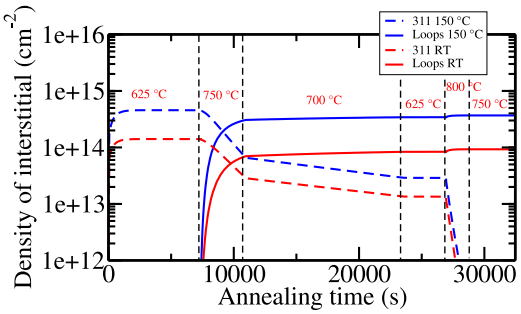

Fig. 3. Number of I trapped in DLs and {311} defects using the hybrid approach combining KMC and continuum model after implantation at RT (red) and at 150 °C (blue). (For interpretation of the references to color in this figure legend, the reader is referred to the web version of this article.)

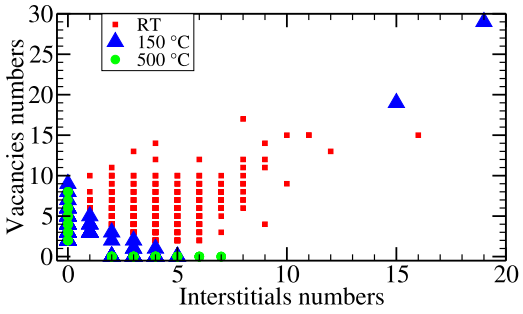

Fig. 4. Histogram of interstitial-vacancies clusters size (size is defined by the number of interstitials and vacancies in a given cluster) after one As implantation and a diffusing step at RT, 150 °C and 500 °C corresponding to two consecutive As collisions in the implantations investigated. The clusters have been averaged on 10 single implantations.

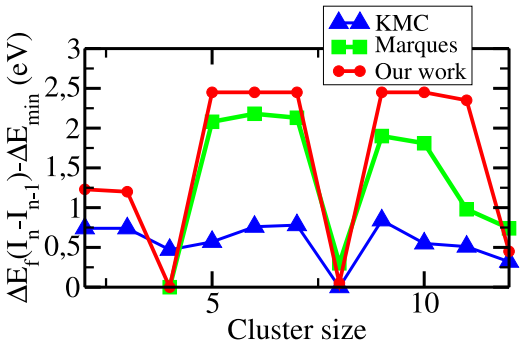

Fig. 5. Difference in formation energies of clusters I_n and I_{n-1} as implemented in the KMC (blue), calculated for the Arai SMIC family using MD [6] (green) and as they were implemented in this work to simulate {311} defects in 500 °C implantation using KMC (red). (For interpretation of the references to color in this figure legend, the reader is referred to the web version of this article.)

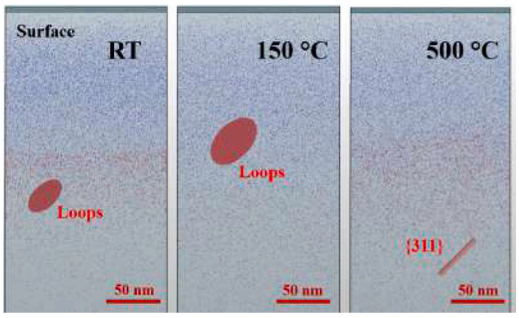

Fig. 6. KMC simulation of RT, 150 °C and 500 °C implantations using updated formation energies as provided in Fig. 5, red curve.

case in KMC simulations. This should lead to a same amount of excess interstitials after interstitial-vacancies recombinations. The difference between the 150 °C and 500 °C implantations should then be caused by the type of clusters where the interstitials are trapped as-implanted and not by a difference in the total interstitials in excess.

To understand what type of defects are formed under the three temperature conditions, we perform a KMC simulation where a single As is implanted in the simulation box using the same dose rate as for the total implantation. The dose rate makes the damaged structures diffuse with a time corresponding to two consecutive As collisions in the used simulation domain. A histogram of the different kinds of amorphous pockets obtained for the three temperature conditions is shown in Fig. 4. It can be observed that in the RT case, interstitials and vacancies are in amorphous pockets containing both vacancies and interstitials with some of them having a size > 10. In the case of 500 °C, interstitials and vacancies are separated and are observed in SMIC-like interstitial clusters or in vacancies clusters, respectively. The behavior observed for a temperature of 150 °C is a mixture between the RT and 500 °C cases: The majority of the clusters are vacancy clusters or SMIC with size < 10 and some bigger clusters containing both interstitials and vacancies are also predicted. Two observations can be made: In the RT and 150 °C case, the larger clusters formed will be more likely to capture additional interstitials in their vicinity when other As particles hit the same region, and larger clusters will be observed compared to the 500 °C case. In the 500 °C implantation, the interstitials are trapped in the SMICs clusters between two collisions and the temperature effects tend to accelerate the formation of the most stable SMICs. On the other hand in the RT and 150 °C implantations, amorphous pockets do not recombine totally and are less likely to form in stable SMICs as-implanted.

SMICs have been the subject of several atomic scale investigations in the literature [6–8]. Two kinds of SMICs have been identified: the chain-like defects type, known as a precursor of {311} [8] and the Arai type whose structure is described in [7]. In the following, we focus on the behavior of Arai type SMICs in the KMC simulation, with a close look on their formation energies and activation energies for emission or association of I as a function of their size.

The Arai type SMIC is known to have very stable structures for I_{4n}. For SMIC size < 6, ab initio calculations of [9] predict that Arai structure has lower formation energies compared to chain-like defect. Looking at the size of SMIC induced by an As implantation at 500 °C in Fig. 4, these SMICs have thus more chances to evolve into Arai structures during the implantation. Moreover the presence of I_4 is believed to limit the growth of SMICs into {311} [10]. The smaller density of interstitials trapped in extended defects in the 500 °C case in the TEM count could be caused by the presence of Arai SMICs as-implanted. In Fig. 6, the KMC model calibrated with energy differences between I_n and I_{n-1} closer to the one calculated in [6] (in Fig. 5) results in the formation of {311} for the 500 °C case and DLs in RT and 150 °C cases (Fig. 6). The formation energy differences between I_n and I_{n-1} are used in the KMC to estimate the activation energy to emit an interstitial from a cluster I_n. This estimate can be improved by further ab initio simulations.

3.4. Contribution of atomistic simulations to the calibration of the KMC

To fit the experimental observations, we observe that the atomistic data are of great help. To support the calibration of atomistic events, notably for the case of I_{4n} and others SMICs, we have carried out an approach combining MD simulations and DFT calculations: The MD simulations allow to identify the stable structures of the system, which are used as input to the DFT for an exact relaxation calculation of the electronic structure of the clusters as well as to determine precisely the activation barriers of the studied mechanisms. This approach is applied

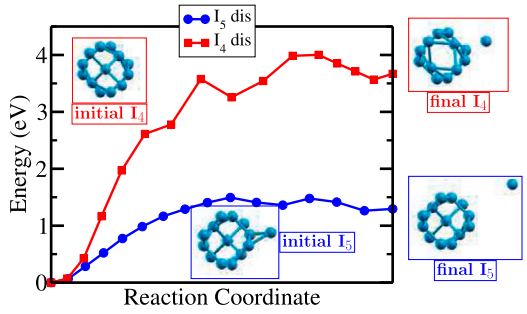

Fig. 7. Minimum energy path between the I_5 configuration and a configuration with an I_4 and an additional interstitial (blue) and minimum energy path between I_4 configuration and configuration with an I_3 and an additional interstitial (red). (For interpretation of the references to color in this figure legend, the reader is referred to the web version of this article.)

here on Arai SMICs of sizes I_4 and I_5 to characterize the activation energy for an interstitial emission.

The MD simulations were performed in a 512 atoms cell and using a Tersoff potential [11] with LAMMPS [12]. The DFT calculations were carried out with Quantum Espresso software [13] on a periodic cell of 512 atoms using a local-density approximation (LDA, Perdew–Zunger). The cut-off energy for the plane waves was set to 20 Ry and the sampling of the reciprocal space was performed at Γ point only. Activation barriers between two relaxed configurations have been determined using ARTn-DFT code [14].

The Arai cluster of type I_5 can be described as an I_4 structure with an additional atom in the near neighborhood bound to two interstitials of the I_4 (see initial I_4 and I_5 structures in Fig. 7). In our calculation, this additional interstitial is chosen to be the emitted atom from the I_5 cluster. In Fig. 7, the minimum energy path is characterized so that the emitted atom from I_5 can be considered as an isolated interstitial at the end of the emission (final I_5 in Fig. 7) and we obtain an energy barrier of the order of 1.5 eV. In Fig. 7, a second smaller barrier is observed in the migration path which corresponds to the activation barrier of the diffusion of an isolated interstitial atom towards a neighboring interstitial site. The emission of an interstitial from an I_4 cluster requires an activation energy of 4.0 eV and results in an I_3 Arai structure with an emitted interstitial (final I_4 in Fig. 7). The energy barrier for the emission of an interstitial is much higher from an I_4 cluster than from an I_5 cluster. However it should be noted that the Arai structure is not the only existing configuration for the I_3 clusters and more complex paths are likely to exist. This result can be compared to the work of [10] in which the barriers to form an I_4 chain-like defect from an Arai structure and the emission energy of an I_4 chain-like structure were calculated. These two mechanisms represent an additional pathway to emit an interstitial from I_4 with an energy barrier of 2.5 eV. These results confirm that the emission of an interstitial from the I_4 Arai structure is much more unlikely than emission from the I_5 Arai structure, as implemented in the calibrated KMC. The evolution of SMICs towards the Arai type during implantation at 500 °C could therefore explain the formation of {311} defects instead of DLs after annealing. Further DFT characterizations of the emission process as a function of SMIC size and type are in progress to better fit Fig. 5.

4. Conclusion

The KMC demonstrates its validity in simulating heated implantation and reproducing experimental observations. For RT and 150 °C, a smart coupling of KMC with continuum model for the simulation of the annealing sequence allows to greatly improve its efficiency. For 500 °C, we show the importance of SMICs stability and of a fine calibration, based on atomic MD and DFT simulations to explain the observed formation of {311} defects.

Declaration of competing interest

The authors declare the following financial interests/personal relationships which may be considered as potential competing interests: Pierre-Louis Julliard reports financial support was provided by MUNDFAB. Pierre-Louis reports a relationship with MUNDFAB that includes: funding grants. Pierre-Louis Julliard has patent pending to 871813. nothing else.

Data availability

The authors do not have permission to share data.

Acknowledgments

The research leading to these results has received funding from the European Union's Horizon 2020 research and innovation program under grant agreement No. 871813 MUNDFAB. This work was performed using HPC resources from CALMIP-Grant P1555 and from TGCC-Genci AD010913556.

References

[1] Nyamhere C, et al. A comprehensive study of the impact of dislocation loops on leakage currents in Si shallow junction devices. J Appl Phys 2015;118(18):184501.
[2] Wen TY, et al. Finfet IO device performance gain with heated implantation. In: 2018 22nd International conference on ion implantation technology. IEEE; 2018, p. 106–9.
[3] Zographos N, et al. Multiscale modeling of doping processes in advanced semiconductor devices. Mater Sci Semicond Process 2017;62:49–61.
[4] Sentaurus Process User Guide, R-2020.09, Synopsys Inc..
[5] Martin-Bragado I, et al. From point defects to dislocation loops: A comprehensive modelling framework for self-interstitial defects in silicon. Solid-State Electron 2008;52(9):1430–6.
[6] Marques LA, et al. {001} Loops in silicon unraveled. Acta Mater 2019;166:192–201.
[7] Arai N, et al. Self-interstitial clustering in crystalline silicon. Phys Rev Lett 1997;78(22):4265.
[8] Kim J, et al. Stability of Si-interstitial defects: From point to extended defects. Phys Rev Lett 2000;84(3):503.
[9] Lee S, et al. Structure and stability of small compact self-interstitial clusters in crystalline silicon. Phys Rev B 2008;77(8):085210.
[10] Du Y, et al. From compact point defects to extended structures in silicon. Eur Phys J B 2007;57(3):229–34.
[11] Tersoff J. Empirical interatomic potential for silicon with improved elastic properties. Phys Rev B 1988;38(14):9902.
[12] Plimpton S. Fast parallel algorithms for short-range molecular dynamics. J Comput Phys 1995;117(1):1–19.
[13] Giannozzi P, et al. QUANTUM ESPRESSO: a modular and open-source software project for quantum simulations of materials. J Phys: Condens Matter 2009;21:395502. http://dx.doi.org/10.1088/0953-8984/21/39/395502.
[14] Jay A, et al. Finding reaction pathways and transition states: r-ARTn and d-ARTn as an efficient and versatile alternative to string approaches. J Chem Theory Comput 2020;16(10):6726–34.